(Received 22 July 2025, Accepted 4 September 2025, Scheduled 13 September 2025)

Deep Learning Assisted Microwave Sensor for Dielectric Material Classification

Sherine Ismail Abd El-Rahman, Hany M. Zamel, and Shimaa A. M. Soliman*

Microwave Engineering Department, Electronics Research Institute (ERI), Cairo, Egypt

ABSTRACT: This paper introduces a deep learning assisted sensor for material classification based on two adjacent split-ring resonators unit cell sensor. This sensor operates in the frequency range from 7 GHz to 8 GHz. The sensor is designed to differentiate between different dielectric materials based on their reflection and transmission properties. A dielectric container is used to hold different samples. Reflection and transmission coefficients for different materials are used for the classification between different dielectric materials. These materials are also characterized by using Dielectric Assessment Kite (DAK) for verification with the proposed method. The Dual Split Ring Resonator (DSRR) unit cell enhanced resonance characteristics facilitate the classification process for distinguishing different dielectric materials. The measured results of the proposed sensor exhibit a broad detection range, accurately identifying various samples based on their unique resonant frequency responses. The proposed sensor finds utility in industrial applications, identifying and categorizing various different dielectric materials. In addition, the proposed design is used to measure a mixture of two different materials with different volume mixing ratios. The measured samples are used to train a convolution neural network to predict the mixing ratio from the measured S-parameters. The combination of this sensor and the trained model is found to be an efficient tool that determines the mixing ratios of different samples in a fast way. This concept can also be useful to be applied on other types of sensors and other sensing parameters.

1. INTRODUCTION

Metamaterials are artificially engineered materials consisting of subwavelength-sized structures, designed to exhibit tailored electromagnetic properties beyond those found in natural materials. The physical properties of metamaterials (MTMs) are highly dependent on the shape, design, orientation, and dimensions of their unit cells. The physical electromagnetic properties of metamaterials are strongly influenced by the geometry, size, and orientation of their constituent unit cells [1, 2]. Split-ring resonators (SRRs) are one type of metamaterial that have been extensively studied for their ability to manipulate electromagnetic waves at microwave and mm-wave frequencies for different applications [1]. On the other hand, complex permittivity of a material represents a critical parameter controlling interaction of electromagnetic waves with the material. This provides a key parameter for material classification. Microwave band enables the realization of much smaller resonators than lower frequencies. On the other hand, the penetration of low-power microwave signals represents surface sensitivity interaction, which is sufficient for material characterization through nondestructive techniques. Planar microwave resonators have attracted significant research interest recently due to their potential for developing real-time material characterization sensors and mixture composition analysis tools, as demonstrated by applications like ethanol-methanol differentiation [3–5].

Pendry et al. proposed a design for metamaterials exhibiting negative permeability based on periodic arrays of coupled SRR [6]. The double SRR structure is characterized by two concentric split-ring resonators, where the smaller ring is situated inside the larger one. This arrangement allows for electromagnetic coupling between the two resonators. The single ring configuration can be modeled by an equivalent RLC resonator, with a resonant frequency of $\omega_0 = 1/\sqrt{LC}$ [7]. The equivalent circuit model of a single ring is just the series connection of an inductor, a capacitor, and a resistor. Double rings with a single metallic slit has mutual inductance and mutual capacitances apart from their inherent RLC parameters. The effective permeability exhibits positive real values below the resonant frequency but exhibits negative value at higher frequencies. When the dimensions of the two rings in double SRRs are very similar, the weak mutual coupling between them creates a behavior close to that of a single SRR with the same overall dimensions. This results in a combined resonance frequency very near that of the single SRR. However, the double SRRs exhibit a larger magnetic moment due to the higher current density concentrated within the smaller ring. The resonant frequency of an SRR is determined by its geometry and material properties. This unique characteristic allows SRRs to operate at a resonant wavelength of 0.1λ, regardless of their dimensions, offering significant miniaturization potential compared to conventional $\lambda/2$ designs [8].

The development of a reusable microwave sensor for non-invasive blood glucose monitoring was presented in [9]. The modified complementary electric LC (CELC) incorporated a

* Corresponding author: Shimaa Ahmed Megahed Soliman (shimaa_megahed@eri.sci.eg).

central cavity, whose sidewalls were coated with a conductive metal layer to enhance capacitance and optimize the interaction between the sensor and the liquid sample contained within the glass capillary.

A method for measuring glucose concentration using a reflective microwave biosensor is described in [10]. This approach introduces a real-time, noninvasive microwave microfluidic sensor designed to measure glucose levels in aqueous solutions. The sensor consists of an open-ended microstrip transmission line integrated with a complementary split-ring resonator (CSRR).

A double split complementary SRR based microwave sensor is proposed in [11] for the high-accuracy measurement of the complex permittivity of liquid samples. The sensor is designed to operate at 2.4 GHz within the industrial, scientific, and medical (ISM) band. The design has been optimized to achieve a significant shift in resonant frequency when liquid samples under test (LUTs) are introduced into contact with the resonator.

Recently, new developments have enabled the development of specialized sensors that can measure different materials characteristics, such as liquids, oils, and powders. The advantageous properties of metamaterial sensors, such as ease of manufacture, compact design, and lower costs for mass production, make them even more popular than conventional sensor systems. The sensitivity of microwave-based sensors for material detection is controlled by the combined effect of the shift in the sensor's resonant frequency induced by the material under test and the variation in the metamaterial's sensitivity based on the different dielectric materials [12–14]. A two-dimensional SRR sensor with a T-shaped geometry is proposed in [15], demonstrating enhanced quality factor compared to traditional SRR designs. An SRR-based microwave sensor enhanced with electromagnetic bandgap (EBG) structure is proposed in [16], leading to a significant improvement in quality factor and enabling accurate measurement of the imaginary part of complex permittivity. The integration of EBG structures into an SRR-based sensor results in a substantial enhancement of quality factor, facilitating the precise measurement of the imaginary component of permittivity. Kiani et al. introduce a planar microstrip sensor for measuring solid material permittivity using a band-stop filter [17]. The interaction between the meandered microstrip resonator and interdigitated structure results in a significant amplification of the electric field within the sensor, enhancing its overall performance for various sensing applications. Wu and Zhao introduce a sensor design based on a magnetic-LC resonator, capable of simultaneously measuring both the thickness and dielectric constant of a material with high accuracy [18]. A double-negative square resonator (DNSRR) sensor, for identifying material thickness and content within the 2–4 GHz range, is presented in [19]. A metamaterial absorber based on a unit cell structure consisting of asymmetric square split rings with a partial E-shaped center resonator is discussed in [20]. The design facilitates enhanced absorption efficiency and improved transmission coefficient through optimized electromagnetic coupling and reduced reflection.

In addition, deep learning becomes a quite efficient tool to model complicated process like discrimination between different physical responses without the need to return to their physical meaning [21]. This can be used to train sensors based on lot of defined measurements to introduce a simple numerical model which is capable to predict the physical parameters for unknown arbitrary measurements. Neural networks based on simple activation functions like rectified linear unit (ReLU) and Sigmoid functions are an efficient tool for developing general simple numerical models. In some cases, a large number of measurement values are required for each process, like measuring S-parameter at different frequencies to determine the dielectric constant of a sample. In this case, it would be better to reduce the number of inputs by extracting the main features in the measurement values. This process is obtained by multiple filterings through convolutional process. This combination is known as Convolutional Neural Network (CNN). The number of layers, number of filters, order of each layer, the used optimization technique, and other parameters determine the efficiency of the proposed model and training convergence [22, 23].

This paper introduces a novel sensor design based on a two-port waveguide section, embedding a DSRR unit cell for enhanced sensitivity and selectivity in material classification within the 7–8 GHz frequency band. The performance of different samples was detected by shifting the resonant frequency, which allowed for the identification of distinct characteristics. The proposed MTM sensor's design and performance were verified through a comprehensive analysis of its surface current, E-field distribution, and equivalent circuit parameters. Then, the designed sensor is used to measure a mixture of cement and sand for different mixing ratios. The measurements are used to develop a CNN model for this senor to directly predict the mixing ratio for the measured S-parameters. The paper is organized as follows. Section 2 outlines the design and simulation of DSRR unit cell sensor. Section 3 introduces the effective complex permeability of the DSRR sensor that was numerically extracted from High Frequency Structure Simulator (HFSS) simulations by employing a rigorous retrieval algorithm. Section 4 presents the equivalent circuit model of the proposed DSRR unit cell. Section 5 introduces the simulated sensor analysis for material classification. Section 6 presents the experimental validation. Then in Section 7, the designed sensor is used to measure different samples of mixture from cement and sand with different volume mixing ratios. These measurements are used to develop a CNN model for predicting the mixing ratio from measured S-parameters. Finally, conclusion is presented in Section 8. The primary innovation of this work lies in the integration of a DSRR for solid mixture sensor for solid mixture with a deep learning model to achieve high-accuracy classification and mixing ratio prediction for dielectric materials, particularly cement-sand mixtures. Table 1 introduces brief comparisons between the proposed sensor and prior works.

2. DESIGN AND SIMULATION OF DSRR UNIT CELL SENSOR

The geometry and dimensions of the proposed DSRR sensor is illustrated in Figure 1. Electromagnetic HFSS was utilized

TABLE 1. Comparison between the proposed sensor and previously published works.

Reference	Focus	Key Limitations Addressed by Our Work
[11] (Beria et al.)	DS-CSRR for liquid permittivity measurement	• Focuses on *liquid samples*; our DSRR targets *solid mixtures* (cement-sand). • Uses traditional resonance-shift analysis; we integrate *end-to-end CNN* for direct mixing ratio prediction.
[14] (Zamel et al.)	Metamaterial sensor for powder classification	• Classifies materials *without quantitative mixing ratios.* • No AI integration; our work adds *regression-based CNN* for volume ratio prediction.
[17] (Kiani et al.)	SRR for solid permittivity measurement	• Measures permittivity *only*; our system predicts *physical mixing ratios* (0–100%). • Uses single-ring resonator; our DSRR enhances sensitivity via dual-ring coupling.
[21] (Li & Salucci)	General DL applications in electromagnetics	• Theoretical overview; we provide a *practical implementation* for industrial mixtures.

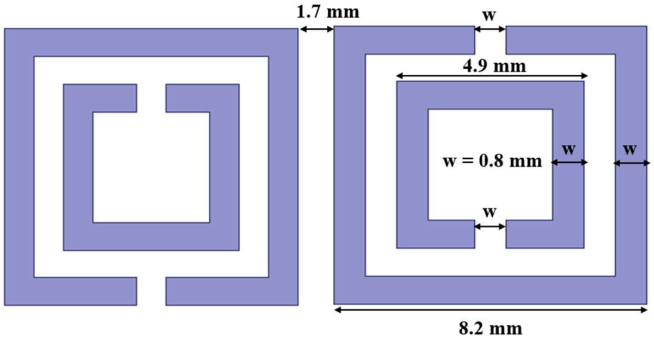

FIGURE 1. Geometry of the proposed antenna.

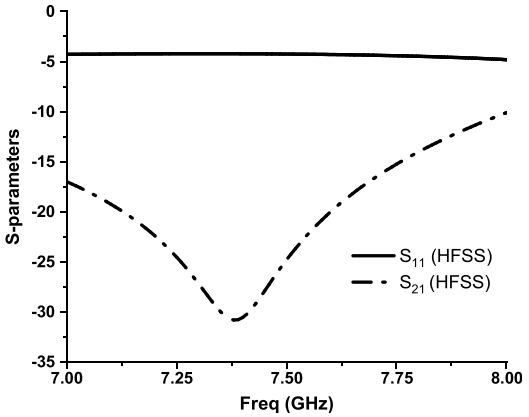

FIGURE 2. Simulated reflection and transmission coefficients for the proposed MTM structure.

for the design and analysis of the DSRR sensor. The suggested DSRR structure mounted on the same side of an FR4 dielectric substrate. The overall dimensions of the MTM sensor are $22.86 \times 10.16\,\text{mm}^2$, which are chosen to match the aperture of the WR90 waveguide. To determine the optimal dimensions for the DSRR unit cell sensor, a parametric analysis is performed to be suitable for the analysis in the frequency region from 7 GHz to 8 GHz. The properties of the used FR4 dielectric substrate include its dielectric constant (ε_r) of 4.3 and loss tangent (tan) of 0.002 with thickness of 1.6 mm. Figure 2 shows the simulated reflection and transmission coefficients for the proposed DSRR unit cell. The minimum transmission of the designed SRR in the range from 7 GHz to 8 GHz can be noted from Figure 2.

3. EXTRACTING THE METAMATERIAL CHARACTERISTICS OF THE PROPOSED DSRR UNIT CELL

The effective complex permeability and permittivity (μ_r, ε_r) of the DSRR sensor were numerically extracted by using complex reflection and transmission coefficients. The permittivity and permeability of the DSRR unit cell are calculated by using the following equations [24, 25]:

$$\varepsilon = \frac{1}{kd}\sqrt{\frac{(1-S_{11})^2 - S_{21}^2}{(1+S_{11})^2 - S_{21}^2}}\cos^{-1}\left[\frac{(1-S_{11}^2+S_{21}^2)}{2S_{21}}\right] \quad (1)$$

$$\mu = \frac{1}{kd}\sqrt{\frac{(1+S_{11})^2 - S_{21}^2}{(1-S_{11})^2 - S_{21}^2}}\cos^{-1}\left[\frac{(1-S_{11}^2+S_{21}^2)}{2S_{21}}\right] \quad (2)$$

The effective parameters (ε, μ) are shown in Figures 3(a) and 3(b). The negative values for permittivity in the frequency range from 7.37 GHz to 7.56 GHz can be noted from Figure 3. On the other hand, the permeability is negative starting from 7.36 GHz and extends to be negative up to the end of the proposed frequency range at 8 GHz.

4. EQUIVALENT CIRCUIT OF THE DSRR UNIT CELL SENSOR

The equivalent circuit model of the proposed DSRR unit cell is represented as two parallel RLC circuits which is connected in series with the capacitor (C_{gab}) that represents the gap capacitance between the two DSRR unit cells, as shown in Figure 4. The lumped elements of the equivalent circuit can be extracted from the corresponding frequency response. The over-

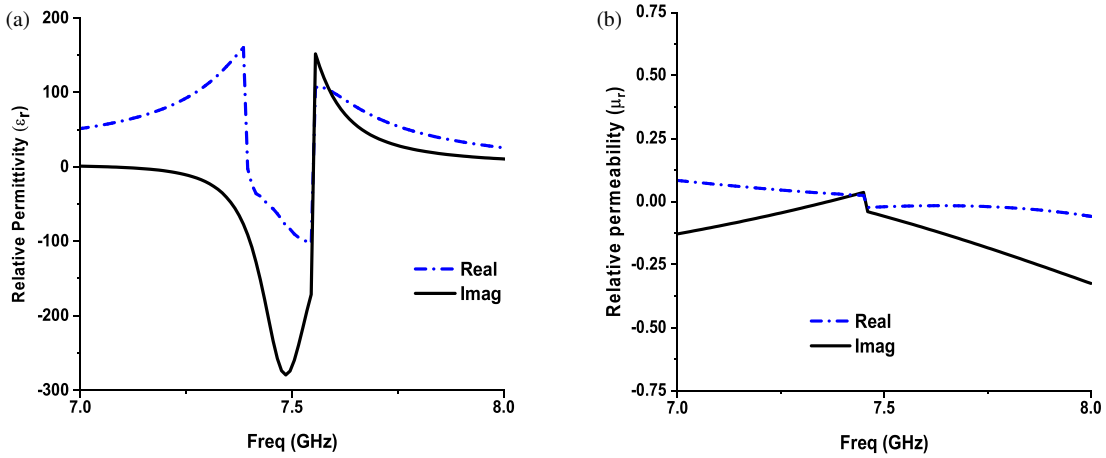

FIGURE 3. (a) Relative permittivity for the proposed SRR structure. (b) Relative permeability for the proposed SRR structure.

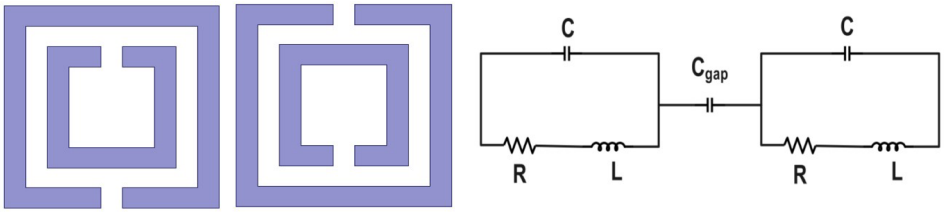

FIGURE 4. Equivalent circuit of unit cell.

all capacitance of the MTM structure depends on the permittivity of the material surrounding it. This sensitivity in capacitance alters the resonance frequency, enabling material characterization and identification through permittivity measurements [26, 27].

The total equivalent resonance frequency is given by [26]:

$$f = \frac{1}{2\pi\sqrt{LC}} \tag{3}$$

where L and C are the total effective inductance and capacitance of the DSRR structure, respectively.

Figure 5 shows the reflection and transmission coefficients of the unit cell and the corresponding equivalent circuit. The results of the unit cell are obtained by using HFSS, and the corresponding ones of the equivalent circuit are obtained by using

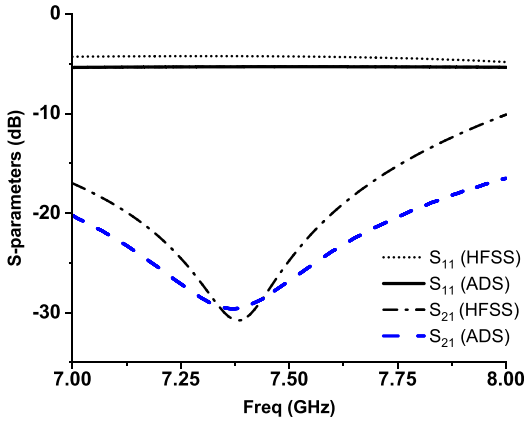

FIGURE 5. Simulated reflection and transmission coefficients for the proposed MTM structure.

TABLE 2. Equivalent circuit parameters.

Parameters	C	R	L	C_{gab}
Values	0.4 pF	2 Ω	1.166 nH	20 pF

Advanced Design System (ADS). Extracted equivalent circuit parameters in this case are listed in Table 2.

5. SIMULATED SENSOR ANALYSIS FOR MATERIAL CLASSIFICATION

The DSRR characterization principle is generally based on the shift in resonant frequency due to the loading materials. This variation in resonant frequency is utilized to differentiate between various materials. MTM unit cell is employed to concentrate the fields within the sample container, thereby enhancing the reflection sensitivity measured by the open-ended waveguide section. The interaction between fields and materials depends on the operating frequency. Thus, the sensing methods also vary depending on the frequency range of applications. Consequently, different sensing methods are implemented across various frequency ranges to exploit this dependence and to achieve optimal material characterization [28, 29].

The classification of different materials samples was simulated without/with a DSRR sensor structure in the frequency range from 7 GHz to 8 GHz. The outputs of the DSRR sensor are influenced by the dielectric constant of sampled positioned inside the sample holder. Figure 6 shows the designed sensor structure (embedded into the waveguide adapter), coinciding with the sample holder position. Effective dimensions of the proposed structure are validated by applying various boundary

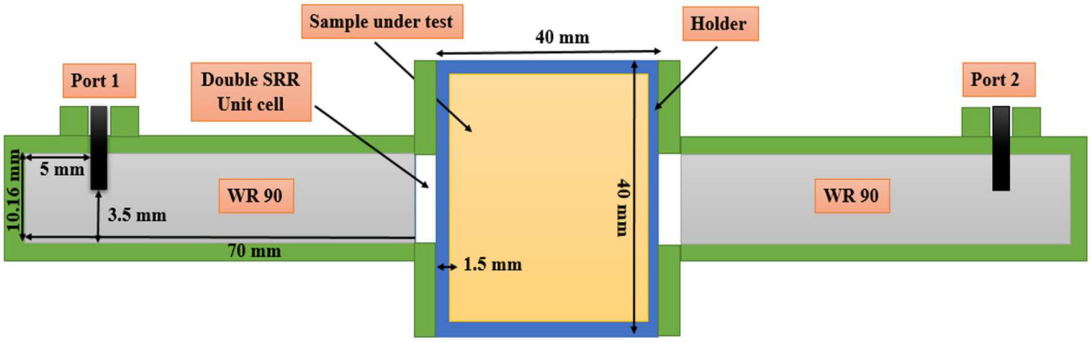

FIGURE 6. System diagram of the microwave sensing process.

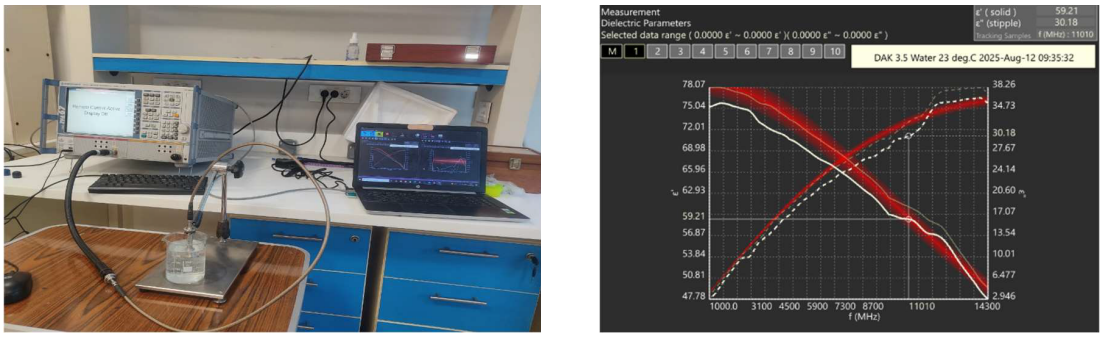

FIGURE 7. Verification of distilled water with DAK.

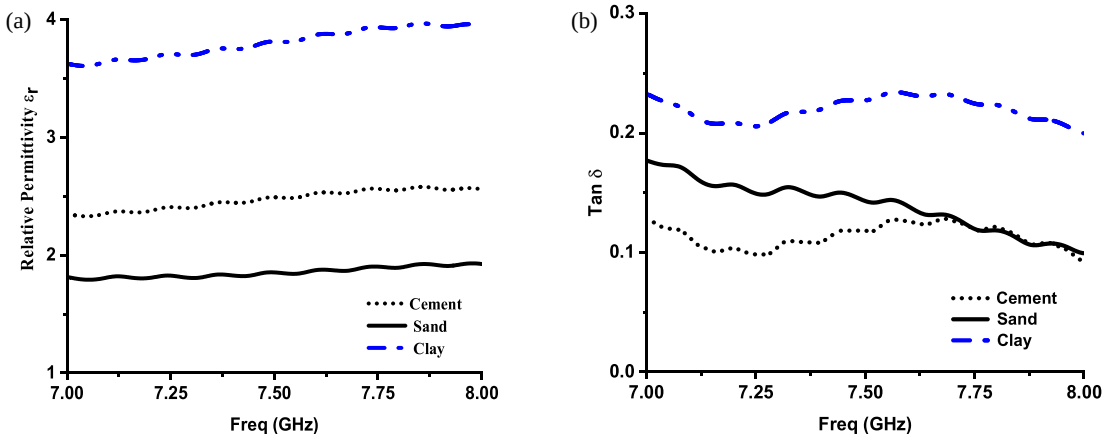

FIGURE 8. Measured permittivity and dielectric constant.

conditions in simulations to match waveguide results. Perfect electrical conductor (PEC) boundary conditions were imposed on the x and y planes during simulations, while open boundaries were assigned to the z-axis and propagation direction. The suggested DSRR structure is placed at the end of the waveguide for validated and experimental analysis [30]. The material under test is placed inside a dielectric container that is attached to open-ended waveguide. A cubic dielectric container with side lengths of 40 mm and a wall thickness of 1.5 mm is made from a material that has a relative permittivity (ε_r) of 3.6.

Samples intended for dielectric measurements must satisfy specific requirements, including adequate volume, homogeneity, and isotropy. The complex permittivity of each sample in terms of the dielectric constant (ε') and dielectric loss factor (ε'') was measured over the frequency range of 5–8 GHz at 25°C. Following calibration using load, open, and short standards, the sample under test was prepared for measurement. Verification of distilled water can be performed for frequencies from 1 GHz to 15 GHz, as shown in Figure 7, and the complex permittivity of water was measured, in terms of the dielectric constant (ε') and dielectric loss factor ε'') at 25°C.

The measured relative permittivity and dielectric loss values of the samples under test at the frequency range of 7 GHz–8 GHz by using a dielectric probe kit are shown in Figures 8(a) and 8(b). Figure 9 shows the simulated transmission coefficient for the proposed unit cell inside waveguide (WG) using Computer Simulation Technology (CST) and HFSS for sand with and without DSRR sensor.

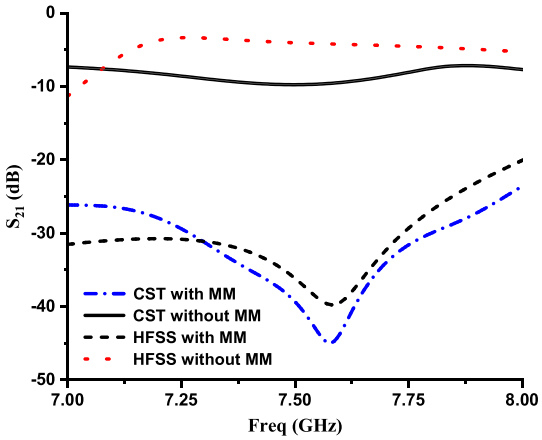

FIGURE 9. Comparative analysis of sand using CST and HFSS simulations, both with and without MTM.

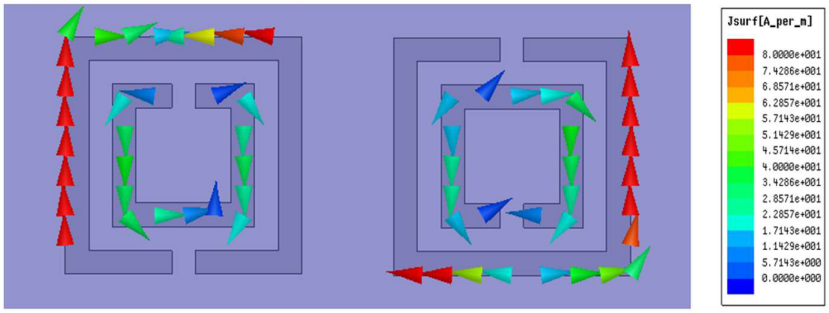

FIGURE 10. Surface current distribution of the microwave DSRR sensor.

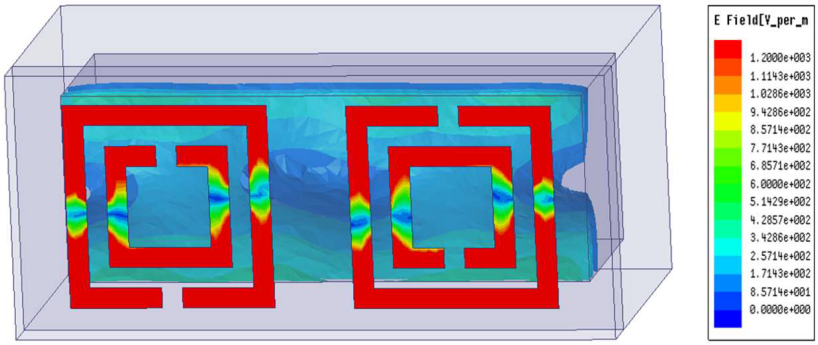

FIGURE 11. Electric field distribution of the microwave DSRR sensor.

Figures 10 and 11 show the electric field and surface current distributions in sand at the resonant frequency of 7.63 GHz, respectively. Examining the distributions of both the electric field and surface current is essential for understanding the operation principles of the proposed sensor. These distributions provide insights into the energy storage and loss mechanisms within the device. When a sample with a different dielectric constant is inserted into the measurement region, it alters the effective permittivity seen by the gaps, thereby modifying the total capacitance in the resonant circuit. Due to the strong field confinement within and around these gaps (as shown in Figure 10 for surface current and Figure 11 for electric field), even small changes in dielectric loading produce noticeable resonance shifts. The outer ring primarily supports stronger current densities, while the inner ring intensifies the electric field in the gap regions, enhancing localized interaction with the sample. This combination of magnetic (from the circulating currents) and electric (from the capacitive gaps) field localization leads to sharper and more distinct resonant responses for different materials. Figure 10 shows the distribution of surface currents along the edges of the DSRR sensor at its resonant frequency of 7.63 GHz for the case of sand. In this case, the current is maximum mainly at the outer rings of the proposed sensor.

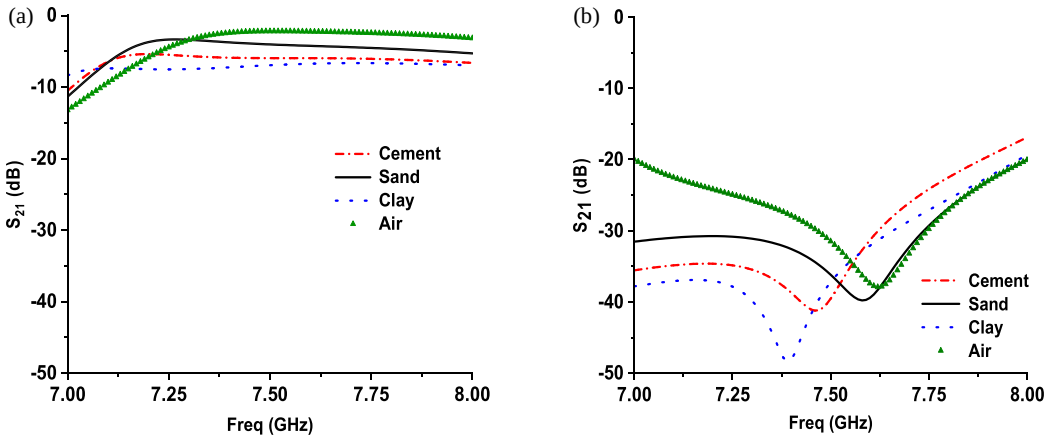

FIGURE 12. Transmission coefficient response of the proposed sensor for different samples without and with the DSRR. (a) Without DSRR. (b) With DSRR.

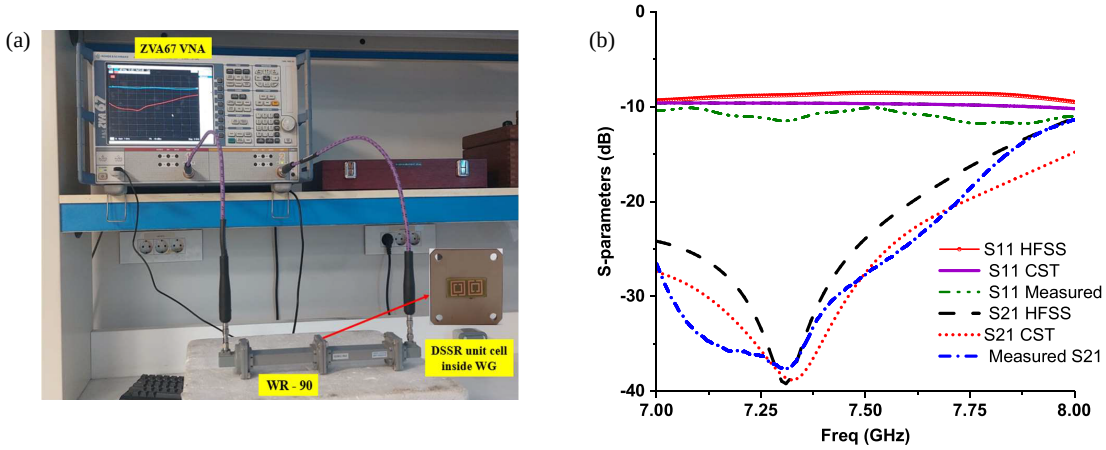

FIGURE 13. (a) Waveguide configuration for the experimental setup. (b) Comparison of measured and simulated results of reflection and transmission coefficient of the MTM unit cell within the waveguide section.

Figure 11 shows the transmission coefficients for the proposed sensor without and with DSRR for different types of materials including cement, sand, clay, and air. It can be noted that the various sample materials without DSRR structure have similar S_{21} peak resonance frequencies, which made it difficult to differentiate them, as shown in Figure 12(a), and the results of samples with MTM are plotted in Figure 12(b). It can be noted that the MTM unit cell significantly improves material classification by generating unique spectral fingerprints for each sample.

6. EXPERIMENTAL VALIDATION

The fabricated sensor structure and experimental setup are depicted in Figure 13(a). Following this configuration, the waveguide is connected to a ZVA67 vector network analyzer (VNA). The reflection and transmission coefficients of the setup based on DSSR are measured and compared with the simulated ones, as shown in Figure 13(b). Good agreement can be noted between measured and simulated results.

Figure 14 shows the proposed material classification setup. The tested materials are initially inserted inside the sample holder. Then, the transmission coefficient is measured. This process is repeated for each measurement step. Due to inherent fabrication and calibration tolerances, minor performance variations were observed.

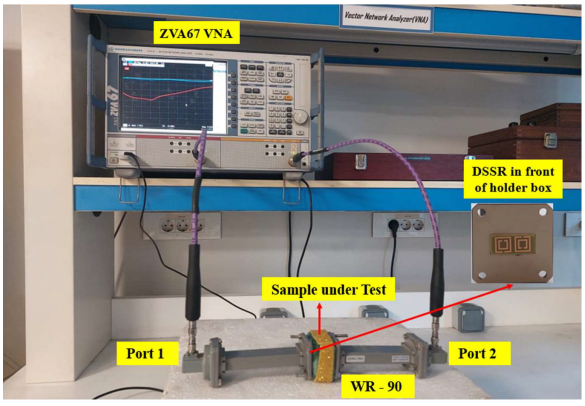

FIGURE 14. System measurements of the microwave sensing process.

The experimental transmission coefficients for different tested materials are presented in Figure 15. It can be noted that the experimental results agree with the simulated ones. It can be noted that without the MTM structure, the measured transmission coefficients are similar for different samples.

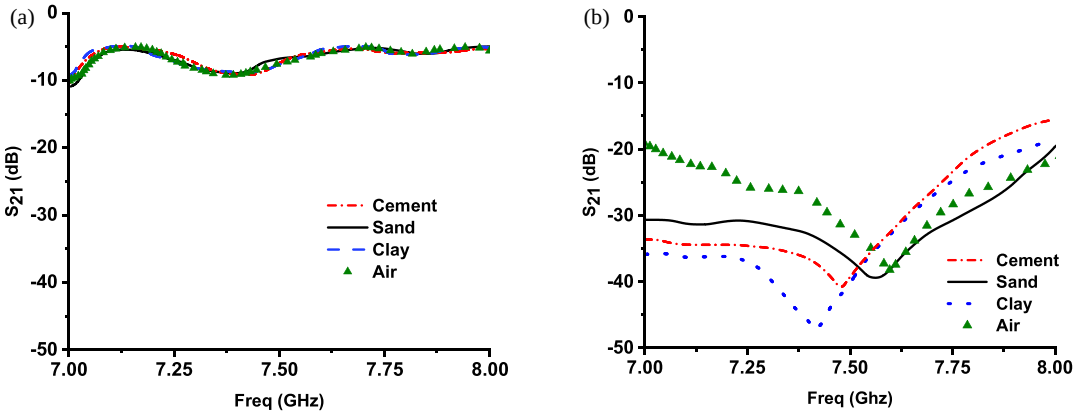

FIGURE 15. Measured S_{21} response: (a) without MTM, (b) with MTM.

TABLE 3. Quantitative classification accuracy table.

	Frequency (GHz)	Transmission coefficient (S_{21}) without DSRR	Transmission coefficient (S_{21}) with DSRR
Cement	7.62	5.95 dB	−37.89 dB
Sand	7.57	4.18 dB	−39.62 dB
Clay	7.45	7.06 dB	−40.70 dB
Air	7.38	2.52 dB	−47.81 dB

TABLE 4. Comparison with other metamaterial-based sensors.

Ref.	Sensing Technique	Size (mm)	Sensing parameters	Resonance frequency (GHz)	Tested Materials	Q-factor	Sensitivity (MHz/ε_r-unit)	FoM
[31]	SRR	45×16	S_{12}	1.72	liquid	43	18	∼774
[32]	SRR	22.86×10.16	S_{11}	9.5	Oils	237.5	25	∼5937
[33]	SRR	40×30	S_{12}	1.85	liquid	46.25	15	∼690
[34]	CSRR	40×40	S_{11}	5.2	Metal	130	N/A	N/A
[35]	patch resonator	88×73	S_{11}, S_{22}	2.430 and 1.950	Metal	60.75/48.75	20	∼1215/∼975
This work	DSRR	22.86×10.16	S_{12}	7.63	Concrete Mix	190.8	42	∼8013.6

This makes it to be challenging to differentiate between the different samples without the MTM structure. In contrast, the MTM unit cell induces distinct transmission coefficient minima for different samples. The observed field enhancement can be attributed to the lensing effect of the MTM unit cell, which concentrates electromagnetic waves onto the materials under test. This enhanced energy concentration within the material allows for more precise differentiation between samples, as varying material properties lead to distinct responses to incident electromagnetic waves.

It is clear in Table 3 that without the MTM (metamaterial) structure, the measured transmission coefficients are almost identical across different samples, making it difficult to distinguish between them. On the other hand, with the presence of MTM it is easy to differentiate the different materials at different resonance frequencies.

Table 4 shows a comparison between the proposed sensor and other previously studied sensors in terms of different performance metrics, including sensing technique, size, parameters, resonant frequency, tested materials, quality factor, sensitivity, and Figure of Merit (FoM). The quality-factor for the proposed sensor is, $Q = fr/\Delta f$, fr is the resonance frequency and Δf is the $+3$ dB bandwidth. For sensing performance characteristic, the FoM is calculated, which is defined as FoM $= S \times Q$, where S is the sensitivity, and Q is the quality factor. The sensitivity is calculated from $S = \Delta f/\Delta\varepsilon_r$.

7. DEEP LEARNING MODEL FOR THE DESIGNED SENSOR

The complete workflow for the material classification system is summarized in Figure 16. The process begins with the de-

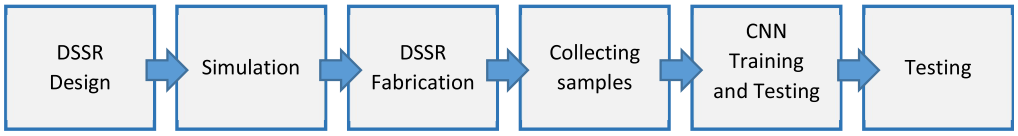

FIGURE 16. Complete workflow for material classification sensor.

sign and simulation of a Double-Square Split Ring (DSSR) resonator, followed by its fabrication. Samples are collected by measuring a comprehensive set of cement-sand mixture samples. The resulting data is used to train and test a Convolutional Neural Network (CNN), which serves as the core intelligent classifier for predicting mixing ratios.

The designed DSRR sensor was employed to measure cement-sand mixtures with volume ratios ranging from 0% to 100% in 1% increments. For each sample, reflection and transmission coefficients S_{11} and S_{21} were recorded at 100 frequency points (7–8 GHz, 10 MHz steps). These measurements were used to train a Convolutional Neural Network (CNN) to predict mixing ratios directly from S-parameters, eliminating manual feature extraction. Below, we will detail the data preprocessing, model architecture, and comprehensive performance evaluation. The designed sensor is used to determine the mixing ratio of cement and sand. To do this, different mixture samples of cement and sand with different mixing ratios are prepared and measured by using the designed sensor. To adjust the mixing ratios, a box with internal dimensions $5 \times 5 \times 4\,\text{cm}^3$ and another box with internal dimensions $1 \times 1 \times 1\,\text{cm}^3$ are prepared to include $100\,\text{cm}^3$ and $1\,\text{cm}^3$ respectively. The first box is completely filled with cement. Then, removing some cement by using the second box to replace it by sand and mixing well, it is possible to get different samples of cement-sand mixtures with volume ratios in steps of 1%. One hundred samples are prepared with volume ratio starting from zero to one. These samples are measured by using the designed sensor, and the corresponding reflection and transmission coefficients are stored. The measurements for each sample are stored for 100 frequency points in the frequency range from 7 to 8 GHz with a step 10 MHz. The design parameters is summarized in Table 5.

TABLE 5. Sample preparation specifications for CNN training dataset.

Parameter	Value
Total Sample Volume	$100\,\text{cm}^3$
Primary Container Dimensions	$5 \times 5 \times 4\,\text{cm}^3$
Incremental Volume	$1\,\text{cm}^3$
Incremental Container Dimensions	$1 \times 1 \times 1\,\text{cm}^3$

These measurements are used to train a Convolution Neural Network (CNN) to develop a model for the response of cement-sand mixture according to the volume ratio of sand to cement. The inputs of this CNN are the S_{11} and S_{21} in dB format. The total number of inputs for each sample is 200. On the other hand, the output of the CNN is the mixing ratio. Fortunately, the mixing ratio lies in the range from 0 to 1, thus, there is no need to normalize it. However, the S parameters in dB format are negative values in the range from -50 to 0 dB. Thus, the first step to use the input data to be suitable for training the proposed CNN is to normalize it to be in the range from 0 to 1. Actually, the magnitude of the S parameters in ratio format is already in the range from to 1, however, the dB format which is based on the logarithmic has a significant variance compared to the direct ratio. This is the reason that the dB format is used combined with normalization. The normalized value is obtained as follows:

$$S_{ij\,\text{normalized}} = \frac{S_{ij\,\text{dB}} + 50}{50} \tag{4}$$

where $S_{ij\,\text{dB}}$ represents either S_{11} or S_{21} in dB format.

The normalized input data for both S_{11} and S_{21} are combined into a single vector of a total length 200. Then, this vector is reshaped to a 2-D matrix of size 20×10. This matrix is passed through three 2-D convolution layers to extract the main features of the input data for each mixing ratio.

The used CNN model shown in Figure 17 consists of:

1. Three 2D Convolutional Layers:
   - Layer 1: 16 filters (3×3 kernel), ReLU activation, max pooling.
   - Layer 2: 32 filters (3×3 kernel), ReLU activation, max pooling.
   - Layer 3: 10 filters (5×2 kernel), ReLU activation.
2. Fully Connected Layers:
   - Four dense layers (64→32→16→1 neurons) with ReLU, except the output layer (sigmoid).

The model was trained using the Adam optimizer (learning rate = 0.001) on 80 samples (80% of data), with 20% reserved for testing.

The performance metrics of the proposed CNN are summarized in Table 6.

The proposed training protocol has a batch size 16 with 200 epochs (of early stopping patience = 15). The Learning rate of Adam optimizer is 0.001. The Loss function is mean squared error. The training time is 22 minutes, and the model is converged at epoch 137. Figure 18 shows the Root Mean Square (RMSE) as a function of the number of training iterations. It can be noted that after 100 iterations the RMSE drops and nearly saturates. The corresponding error loss is shown in Figure 19. After that, the trained network is stored. This stored network is used to predict the volume ratios for different samples in the range from to 1. In this case, the measured S-parameters are

TABLE 6. Performance metrics of the proposed CNN.

Metric	Value	Interpretation
Root Mean Squared Error (RMSE)	0.042	Error $< 4.2\%$ of output range.
Mean Absolute Error (MAE)	0.035	Average deviation $\pm 3.5\%$.
R^2 (Coefficient of Determination)	0.983	Near-perfect fit ($1.0 =$ ideal).
Max Absolute Error	0.089	Worst-case error $< 8.9\%$.

Cross-Validation: 5-fold CV yielded consistent results (mean RMSE $= 0.045 \pm 0.003$), confirming robustness.

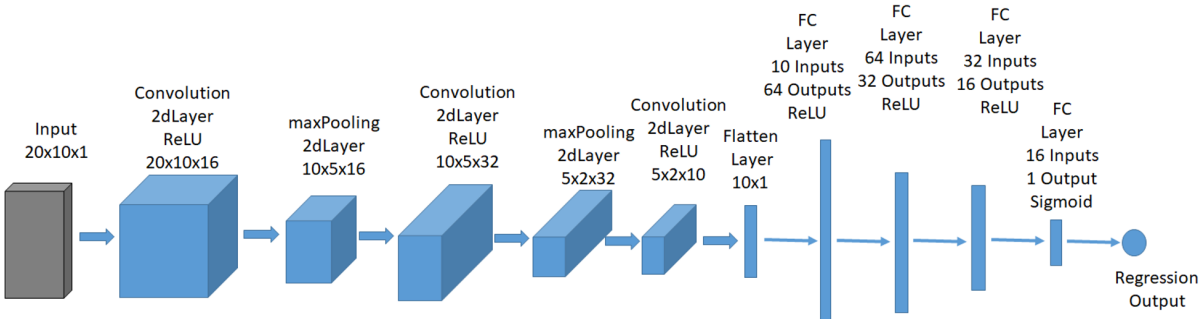

FIGURE 17. Structure of the proposed Convolution Neural Network.

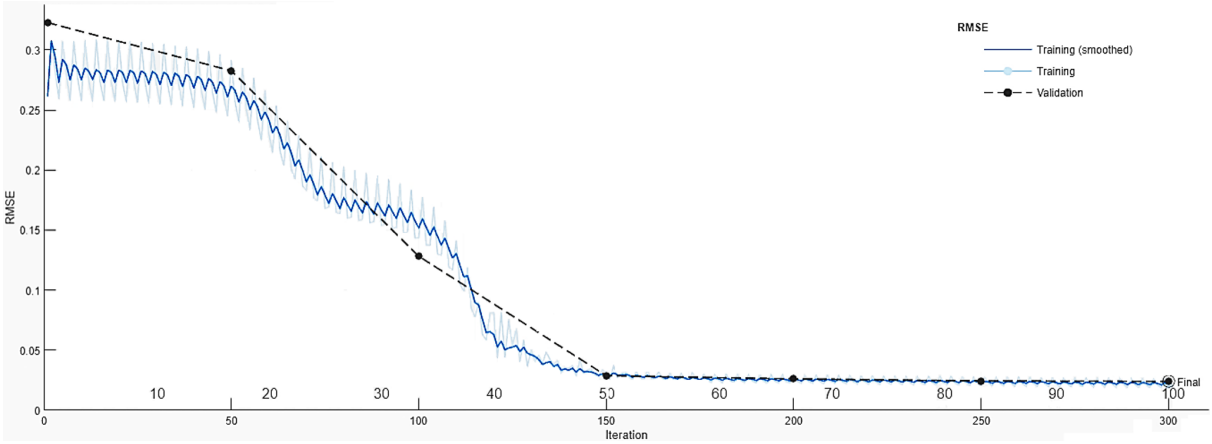

FIGURE 18. Root Mean Square Error (RMSE) of the training process as number of iterations.

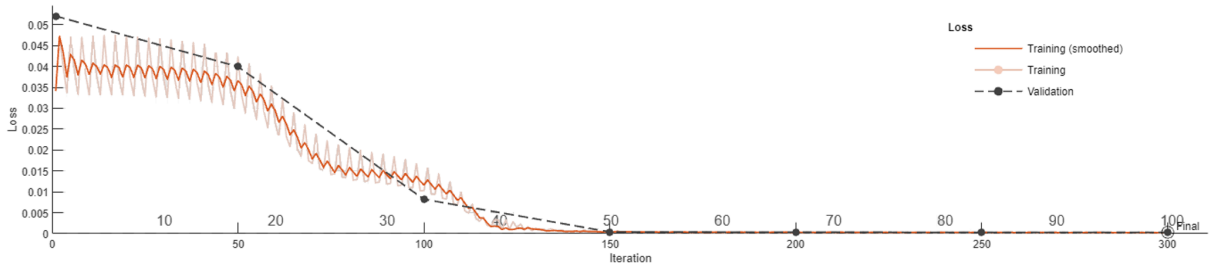

FIGURE 19. Loss values of the training process as number of iterations.

used as inputs to the trained network which introduce the predicted volume ratio. Figure 20 shows a comparison between the actual volume ratios and obtained predicted values. Good agreement between the actual and predicted values is obtained as shown in Figure 20. These results indicate the applicability of using the designed sensor combined with the trained model to predict the volume ratio of a mixture for cement and sand.

The trained model predicts mixing ratios in real time (inference time $=$ 2.1 ms/sample on an Intel i7 CPU), enabling rapid quality control for construction materials. This approach is generalizable to other mixtures (e.g., polymers, pharmaceu-

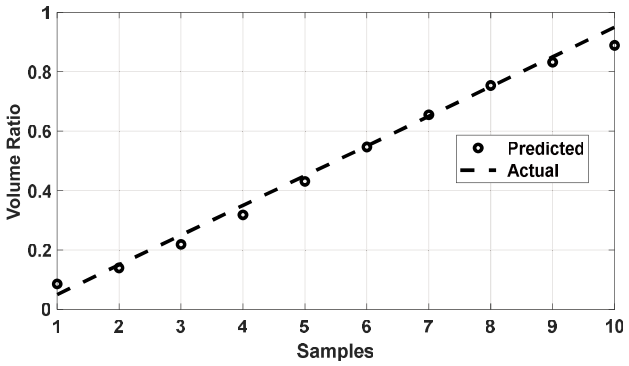

FIGURE 20. Comparison between actual ratios and predicted ratios by using the trained model. Actual values are presented by dashed line and predicted values are presented by circles.

ticals) by retraining CNN with new data. The same problem is modeled by using other Deep Learning (DL) models. Comparisons between the performance of the proposed CNN model and other models are summarized in Table 7. It can be noted that the proposed CNN has more efficient performance than other techniques.

TABLE 7. Comparison between the proposed CNN and other DL models.

Mode	RMSE	MAE	R^2	Training Time
CNN (Proposed)	0.042	0.035	0.983	22 min
Random Forest	0.068	0.052	0.941	8 min
SVM (RBF)	0.095	0.078	0.884	12 min
Linear Regression	0.112	0.091	0.871	2 min

8. CONCLUSION

In this paper, a DSRR unit cell sensor is proposed for the classification of different samples in the frequency range from 7 GHz to 8 GHz. The classification accuracies of powder samples, both with and without a DSRR structure, were studied by using HFSS and CST. In addition, the equivalent circuit of the DSRR unit cell sensor was developed using ADS. The frequency-shifting feature allows the sensor to achieve enhanced sensitivity in distinguishing between different samples. The obtained measured resonance frequencies with MTM are 7.48 GHz, 7.56 GHz, 7.42 GHz, and 7.59 GHz for samples (cement, sand, clay, and air, respectively). The measured results have good agreements with the simulated ones, which validates the potential applications of the proposed DSRR unit cell sensor for different samples. This sensor is used to measure different samples of mixtures composed of cement and sand with different volume ratios. These measured samples are used to train a CNN model. The trained CNN model combined with the designed sensor is found to be an efficient tool and determine the ratio of cement-sand mixtures for different volume ratios in the range from to 1. The proposed technique can also be useful for other sensing techniques.

ACKNOWLEDGEMENT

The authors would like to express their deepest gratitude to Prof. Ahmed M. Attiy (Microwave Engineering Department, ERI), for his invaluable guidance, insightful feedback, and constant encouragement to develop this work.

REFERENCES

[1] Veselago, V. G., "The electrodynamics of substances with simultaneously negative values of ε and μ," *Soviet Physics Uspekhi*, Vol. 10, No. 4, 509–514, 1968.

[2] Sim, M. S., K. Y. You, R. Dewan, F. Esa, M. R. Salim, C. S. Khe, S. Y. N. Kew, and F. Hamid, "Microwave sensors loaded with metamaterial-inspired resonators for dielectric material characterization: A review," *Sensors and Actuators A: Physical*, Vol. 372, 115322, 2024.

[3] Muñoz-Enano, J., P. Vélez, M. Gil, and F. Martín, "Planar microwave resonant sensors: A review and recent developments," *Applied Sciences*, Vol. 10, No. 7, 2615, 2020.

[4] Alahnomi, R. A., Z. Zakaria, Z. M. Yussof, A. A. Althuwayb, A. Alhegazi, H. Alsariera, and N. A. Rahman, "Review of recent microwave planar resonator-based sensors: Techniques of complex permittivity extraction, applications, open challenges and future research directions," *Sensors*, Vol. 21, No. 7, 2267, 2021.

[5] Van Dijck, M., M. Chavoshi, H. Ponsaerts, T. Markovic, and D. Schreurs, "Complex permittivity extraction for ethanol-water mixtures characterization using artificial neural networks," in *2023 IEEE MTT-S International Microwave Biomedical Conference (IMBioC)*, 151–153, Leuven, Belgium, 2023.

[6] Pendry, J. B., A. J. Holden, D. J. Robbins, and W. J. Stewart, "Magnetism from conductors and enhanced nonlinear phenomena," *IEEE Transactions on Microwave Theory and Techniques*, Vol. 47, No. 11, 2075–2084, 1999.

[7] Caloz, C. and T. Itoh, *Electromagnetic Metamaterials: Transmission Line Theory and Microwave Applications*, John Wiley & Sons, Inc., 2005.

[8] Brito, D. B., H. C. C. Fernandes, A. G. D'Assunção, and X. Begaud, "Complementary split ring resonator stop-band filter for UWB applications," in *2011 SBMO/IEEE MTT-S International Microwave and Optoelectronics Conference (IMOC 2011)*, 697–700, Natal, Brazil, 2011.

[9] Govind, G. and M. J. Akhtar, "Design of an ELC resonator-based reusable RF microfluidic sensor for blood glucose estimation," *Scientific Reports*, Vol. 10, No. 1, 18842, 2020.

[10] Ebrahimi, A., J. Scott, and K. Ghorbani, "Microwave reflective biosensor for glucose level detection in aqueous solutions," *Sensors and Actuators A: Physical*, Vol. 301, 111662, 2020.

[11] Beria, Y., G. S. Das, A. Buragohain, and B. B. Chamuah, "Highly sensitive miniaturized octagonal DS-CSRR sensor for permittivity measurement of liquid samples," *IEEE Transactions on Instrumentation and Measurement*, Vol. 72, 1–9, 2023.

[12] Javadizadeh, S., M. Badieirostami, and M. Shahabadi, "Ultra-sensitive miniaturized planar microwave sensor for characterization of water-alcohol mixtures," *Scientific Reports*, Vol. 13, No. 1, 14144, 2023.

[13] Martín, F., P. Vélez, J. Muñoz-Enano, and L. Su, *Planar Microwave Sensors*, 1st ed., John Wiley & Sons, Inc., 2023.

[14] Zamel, H. M., S. I. A. El-Rahman, and A. M. Attiya, "Metamaterial enhanced sensor for powder material classification," *Scientific Reports*, Vol. 14, No. 1, 21316, 2024.

[15] Navaei, M., P. Rezaei, and S. Kiani, "Microwave split ring resonator sensor for determination of the fluids permittivity with

measurement of human milk samples," *Radio Science*, Vol. 57, No. 7, 1–11, 2022.

[16] Jahangiri, P., M. Naser-Moghadasi, B. Ghalamkari, and M. Dousti, "A new planar microwave sensor for fat-measuring of meat based on SRR and periodic EBG structures," *Sensors and Actuators A: Physical*, Vol. 346, 113826, 2022.

[17] Kiani, S., P. Rezaei, M. Navaei, and M. S. Abrishamian, "Microwave sensor for detection of solid material permittivity in single/multilayer samples with high quality factor," *IEEE Sensors Journal*, Vol. 18, No. 24, 9971–9977, 2018.

[18] Wu, W.-J. and W.-S. Zhao, "A differential microwave sensor loaded with magnetic-LC resonators for simultaneous thickness and permittivity measurement of material under test by odd- and even-mode," *IEEE Sensors Journal*, Vol. 23, No. 12, 12 808–12 816, 2023.

[19] Khalil, M. A., W. H. Yong, M. T. Islam, A. Hoque, M. S. Islam, C. C. Leei, and M. S. Soliman, "Double-negative metamaterial square enclosed QSSR for microwave sensing application in S-band with high sensitivity and Q-factor," *Scientific Reports*, Vol. 13, No. 1, 7373, 2023.

[20] Rabbani, M. G., M. T. Islam, A. Hoque, B. Bais, S. Albadran, M. S. Islam, and M. S. Soliman, "Orthogonal centre ring field optimization triple-band metamaterial absorber with sensing application," *Engineering Science and Technology, An International Journal*, Vol. 49, 101588, 2024.

[21] Li, M. and M. Salucci, *Applications of Deep Learning in Electromagnetics: Teaching Maxwell's Equations to Machines*, IET, 2023.

[22] Martínez-Ramón, M., A. Gupta, J. L. Rojo-Álvarez, C. Christodoulou, and K. Cools, "Machine learning applications in electromagnetics and antenna array processing [book review]," *IEEE Antennas and Propagation Magazine*, Vol. 64, No. 4, 178–179, 2022.

[23] Christodoulou, C. and M. Georgiopoulos, *Applications of Neural Networks in Electromagnetics*, Artech House, 2000.

[24] Smith, D. R., D. C. Vier, T. Koschny, and C. M. Soukoulis, "Electromagnetic parameter retrieval from inhomogeneous metamaterials," *Physical Review E*, Vol. 71, No. 3, 036617, 2005.

[25] Islam, M. T., *Metamaterial for Microwave Applications*, 1st ed., CRC Press, 2023.

[26] Marqués, R., F. Mesa, J. Martel, and F. Medina, "Comparative analysis of edge- and broadside-coupled split ring resonators for metamaterial design — Theory and experiments," *IEEE Transactions on Antennas and Propagation*, Vol. 51, No. 10, 2572–2581, 2003.

[27] Marqués, R., F. Medina, and R. Rafii-El-Idrissi, "Role of bianisotropy in negative permeability and left-handed metamaterials," *Physical Review B*, Vol. 65, No. 14, 144440, 2002.

[28] Ebrahimi, A., J. Scott, and K. Ghorbani, "Transmission lines terminated with LC resonators for differential permittivity sensing," *IEEE Microwave and Wireless Components Letters*, Vol. 28, No. 12, 1149–1151, 2018.

[29] Haq, T. and S. Koziel, "Novel complementary resonator for dielectric characterization of substrates based on permittivity and thickness," *IEEE Sensors Journal*, Vol. 24, No. 1, 195–203, 2024.

[30] Abdulkarim, Y. I., L. Deng, H. Luo, S. Huang, M. Karaaslan, O. Altıntaş, M. Bakır, F. F. Muhammadsharif, H. N. Awl, C. Sabah, and K. S. L. Al-Badri, "Design and study of a metamaterial based sensor for the application of liquid chemicals detection," *Journal of Materials Research and Technology*, Vol. 9, No. 5, 10 291–10 304, 2020.

[31] Ye, W., D.-W. Wang, J. Wang, G. Wang, and W.-S. Zhao, "An improved split-ring resonator-based sensor for microfluidic applications," *Sensors*, Vol. 22, No. 21, 8534, 2022.

[32] Islam, M. R., M. T. Islam, M. Salaheldeen, B. Bais, S. H. A. Almalki, H. Alsaif, and M. S. Islam, "Metamaterial sensor based on rectangular enclosed adjacent triple circle split ring resonator with good quality factor for microwave sensing application," *Scientific Reports*, Vol. 12, No. 1, 6792, 2022.

[33] Galindo-Romera, G., F. J. Herraiz-Martínez, M. Gil, J. J. Martínez-Martínez, and D. Segovia-Vargas, "Submersible printed split-ring resonator-based sensor for thin-film detection and permittivity characterization," *IEEE Sensors Journal*, Vol. 16, No. 10, 3587–3596, 2016.

[34] Pawde, S. and N. Gupta, "Microwave sensors for metal conductivity measurement," *Microwave Review*, Vol. 30, No. 1, 16–22, 2024.

[35] Qian, B., L. Mou, L. Wu, Z. Xiao, T. Hu, and J. Jiang, "A direction-sensitive microwave sensor for metal crack detection," *Applied Sciences*, Vol. 12, No. 18, 9045, 2022.